Biochimica et Biophysica Acta 1828 (2013) 1181–1191

Contents lists available at SciVerse ScienceDirect

Biochimica et Biophysica Acta

journal homepage: www.elsevier.com/locate/bbamem

K^+-induced conformational changes in the trimeric betaine transporter BetP monitored by ATR-FTIR spectroscopy ☆

Filiz Korkmaz [a,b], Susanne Ressl [c], Christine Ziegler [d,e,*], Werner Mäntele [a,**]

[a] Institute for Biophysics, Goethe-University, Max-von-Laue Str.1 D-60438, Frankfurt am Main, Germany
[b] Atılım University, Faculty of Engineering, Physics Unit, 06836, İncek, Ankara, Turkey
[c] Stanford University, Howard Hughes Medical Institute, Department of Molecular & Cellular Physiology, Stanford, CA 94305, USA
[d] Max Planck Institute of Biophysics, Department of Structural Biology, Max-von-Laue-Str. 3, D-60438, Frankfurt am Main, Germany
[e] Institute of Biophysics, University of Regensburg, Universitätsstr. 31, D-93051 Regensburg, Germany

ARTICLE INFO

Article history:
Received 24 September 2012
Received in revised form 10 December 2012
Accepted 8 January 2013
Available online 11 January 2013

Keywords:
Secondary transporter
BetP
Transport regulation
Side chain subtraction
Secondary structure
Curve fitting

ABSTRACT

The trimeric Na^+-coupled betaine symporter BetP from *Corynebactrium glutamicum* adjusts transport activity according to the external osmolality. BetP senses the increasing internal K^+ concentration, which is an immediate consequence of osmotic upshift in *C. glutamicum*. It is assumed that BetP specifically binds potassium to yet unidentified binding sites, thereby inducing conformational changes resulting in activation. Atomic structures of BetP were obtained in the absence of potassium allowing only a speculative glimpse on a putative mechanism of K^+-induced transport activation. The structural data suggest that activation in BetP is crucially linked to its trimeric state involving an interaction network between several arginines and glutamates and aspartates. Here, we describe the effect of K^+-induced activation on the specific ionic interaction sites in terminal domains and loops and on the protomer–protomer interactions within the trimer studied by ATR-FTIR spectroscopy. We suggest that arginine and aspartate and/or glutamate residues at the trimeric interface rearrange upon K^+-induced activation, although they remain assembled in an interaction network. Our data propose a two-step mechanism comprising first a change in solvent exposure of charged residues and second a modification of their interaction sites in a partner-switching manner. FTIR reveals a higher α-helical content than expected from the X-ray structures that we attribute to the structurally unresolved N-terminal domain modulating regulation. In situ $^1H/^2H$ exchange studies point toward an altered exposure of backbone regions to buffer solution upon activation, most likely due to conformational changes in both terminal domains, which further affects ionic interactions within the trimer.

© 2013 Elsevier B.V. All rights reserved.

1. Introduction

BetP from the soil bacterium *Corynebacterium glutamicum* is a secondary betaine transporter of the Betaine–Choline–Carnitine Transporter (BCCT) family [1–3]. It couples the transport of two Na^+ ions to the uptake of one betaine molecule. Betaine is an efficient osmolyte that is accumulated to high intracellular amounts by BetP in response to an up-shift in the external osmolality [1]. BetP is activated above ~200 mOsmol/kg in *C. glutamicum* cells [4,5] triggered by an increase in internal K^+ concentration as a consequence of immediate cell shrinkage [6].

The positively charged C-terminal domain was identified as a K^+-sensor [7]. Regulatory properties of BetP depend strongly on the surrounding membrane, e.g., on the presence of negatively charged lipids [8], a concept that was also observed for other osmoregulated transporters such as the ABC transporter OpuA from *Lactococcus lactis* [9]. However, the strict activation specificity by potassium ions is a unique feature of BetP.

The atomic structure revealed that BetP shares a LeuT-like fold of two inverted, topology-related repeats of 5 transmembrane helices[1] (TMH) [10] (Fig. 1). Helices from both repeats contribute to an iris-shaped 4-TMH bundle and a C-shaped scaffold of 6-TMH (Fig. 1), which form a tightly packed 10-TMH transporter core. In BetP, conformational changes involve a gating-like flexing mechanism of periplasmic ends of TMH8 and TMH12 and of the cytoplasmic ends of TMH3 and TMH7 together with a bending of TMH5 and TMH10, which are both involved in the coordination of sodium ions [11]. In addition, BetP comprises an amphiphatic helix (H7) that runs parallel to the periplasmic membrane linking both repeats.

Abbreviations: TMH, transmembrane helix; ATR-FTIR, attenuated total reflection Fourier transform infrared spectroscopy; LB, lysogeny broth; DDM, β-Dodecyl-maltoside; KPi, potassium phosphate; RMS, root mean square; EPR, electron paramagnetic resonance; AFM, atomic force miscroscopy; a.a., amino acid

☆ This work was supported by the Deutsche Forschungsgemeinschaft (SFB 472 and SFB 807).

* Correspondence to: C. Ziegler, Max Planck Institute of Biophysics, Department of Structural Biology, Max-von-Laue-Str. 3, D-60438, Frankfurt am Main, Germany. Tel.: +49 69 6303 3054; fax: +49 69 6303 3002.
** Corresponding author. Tel.: +49 69 798 46410; fax: +49 69 798 46423.
E-mail addresses: Christine.Ziegler@biophys.mpg.de (C. Ziegler), maentele@biophysik.uni-frankfurt.de (W. Mäntele).

0005-2736/$ – see front matter © 2013 Elsevier B.V. All rights reserved.
http://dx.doi.org/10.1016/j.bbamem.2013.01.004

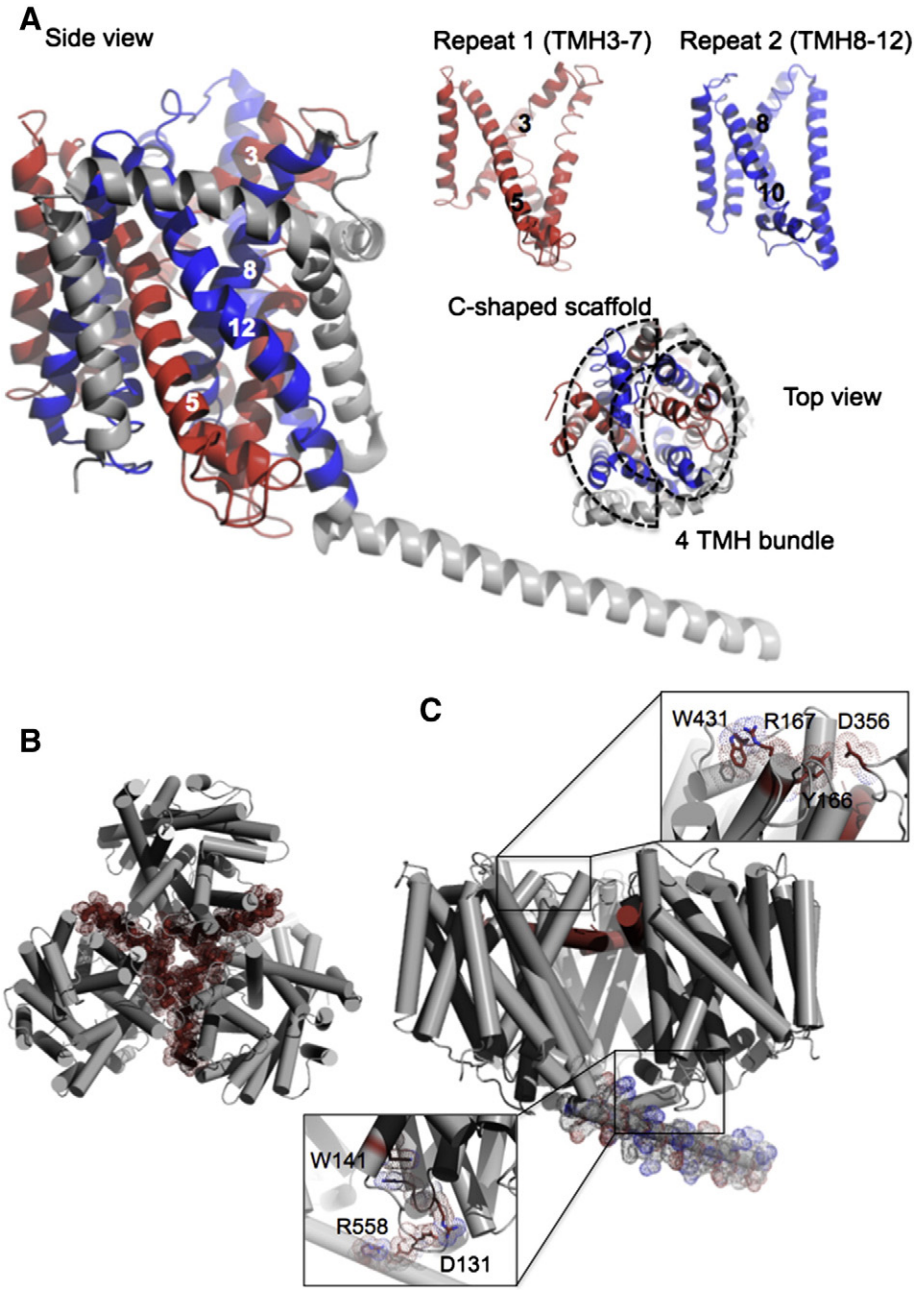

Fig. 1. (A) Side view on a BetP monomer. The two structural repeats are colored in red and blue and form the 10 TMH transporter core consisting of a 4 TMH bundle and a C-shaped scaffold of 6 TMH. The repeats are inverted with respect to each other. (B) Top view of a BetP trimer from the periplasmic side. The main trimerization contacts are formed by residues located in H7 (red) and TMH 2. (C) Intratrimeric interaction networks on the periplasmic side (top inset) and on the cytoplasmic side (bottom inset) depicted in a side view on two BetP protomers. On the cytoplasmic side, Arg558 in the C-terminal domain interacts with Asp131 in loop2 of the counterclockwise adjacent protomer. The neighbor Glu132 interacts with Arg390 of loop8, which subsequently positions Arg392 in this loop to maintain a cation-π interaction with Trp141 in TM3. On the periplasmic side of BetP, Asp356 in loop7 is interacting with Tyr166 in loop3 of the clockwise adjacent protomer and thereby facilitating a cation-π interaction of Arg167 located in the cytoplasmic end of TM3 with Trp431 in loop9. Both networks are in close proximity to TM3, which coordinates coupled binding of betaine and sodium (11) and link all three protomers together.

This helix contains the main trimerization contact sites (Fig. 1B, top view) and provides a platform for two intratrimeric ionic interaction networks (Fig. 1C, side view and insets). In the trimeric assembly, the C-terminal domain of each protomer is interacting with cytoplasmic loops of the adjacent protomer [12]. This ionic interaction is maintained by positively charged residues located in the C-terminal domain (Arg552-Arg568) and a negatively charged residue located in loop2 (Asp131) (Fig. 1C). A second ionic network between loop2 (Glu132) and loop8 (Arg390) transduces the cytoplasmic intratrimeric interactions to bundle helices that are key players in the alternating-access mechanism of BetP [11]. Nearly all residues in the α-helical C-terminal domain between Tyr550 to Ala580 are critical in K^+ sensing and activation, and any point mutation disturbing the helical motif results in deregulation of BetP [13]. A similar ionic interaction network was identified at the periplasmic side contributing to the stability of H7 [14] (Fig. 1C, inset). A cation-pi interaction between Arg167 and Trp431 is linked here to the interaction of Tyr166 with Asp356 from the adjacent protomer. Although structural and functional data suggest the impact of the C-terminal domain and H7 on regulation, only little is known on how these elements dynamically change their conformation upon K^+-induced activation. Recently, studies on single molecule force spectroscopy [15] and EPR [16] have shed some light on the dynamical process of BetP activation. The crucial question remains whether

K^+-binding to BetP will result in major re-arrangements of these networks or even of the trimeric architecture and how different are the active and inactive conformation in BetP.

Here, we investigate the effect of K^+- activation on the conformational state of distinct structural elements of BetP, in particular intratrimeric and intramolecular interactions, by attenuated total reflection (ATR)-FTIR spectroscopy [17–21]. We have used a specifically developed ATR-FTIR microdialysis cell [22], which enabled us to track changes in protein secondary structure, to monitor side chain interactions and to perform $^1H/^2H$ exchange upon K^+-induced activation. Moreover, close-to-natural conditions in the absence of any restricting crystal contacts and conformational changes upon activation can be scanned simultaneously [22–26].

2. Experimental procedures

2.1. Protein expression and purification

Escherichia coli DH5 αmcr [27] was used for the heterologous expression of strep-*betP*. Cells were grown at 37 °C in LB medium supplemented with carbenicillin (50 μg/ml) and induction was initiated with anhydrotetracycline (200 μg/l). Cells were harvested at 4 °C by centrifugation and resuspended in buffer containing 100 mM Tris–HCl (pH 8) and protease inhibitor Pefabloc at 0.2 mg/ml. Membranes were isolated from disrupted cells and solubilized with 2.5% β-dodecyl-maltoside (DDM). The protein was then loaded on a StrepII-Tactin macroprep® column, washed with 50 mM Tris–HCl (pH 7.5), 500 mM NaCl, 8.6% Glycerol, 0.05–0.1% DDM, and eluted with 5 mM desthiobiotin, 50 mM Tris–HCl (pH 7.5), 200 mM NaCl, 8.7% glycerol and 0.05% DDM. Prior to FTIR measurements the protein was loaded onto a Superose 6 (GE Healthcare) size-exclusion column equilibrated with 20 mM Tris–HCl (pH 7.5), 200 mM NaCl and 0.1% DDM and concentrated at 4 °C to approx. 10 mg/ml at 3000 g in a Vivaspin tube (Vivascience) with a 100 k-molecular-weight cut-off.

2.2. ATR-FTIR measurements

5 μl of purified, detergent-solubilized protein sample (0.1 mM final concentration) was placed on the diamond ATR cell of a Bruker VECTOR 22 FTIR- Spectrometer (Bruker Optics, Ettlingen, Germany), equipped with an MCT detector. The protein compartment of this perfusion ATR cell was separated from the perfusion buffer by a dialysis membrane with cut-off at 25 kDa. Details of the perfusion microcell have been described elsewhere [22]. 0.1 M potassium phosphate (KP_i) buffer, pH 7.4 with 0.1% n-dodecyl beta-D-maltoside (DDM) was perfused for at least 2 h across the protein sample to change the buffer of the purified protein. The perfusion rate was set to ~1.5 ml/min. 0.1 M KP_i buffer, p^2H 7.4, 0.1% DDM buffer including 0.5 M NaCl was then perfused for 24 h in order to ensure maximal deuterium exchange. A total of 256 scans were averaged and Fourier-transformed using a zero-filling factor for a spectral resolution of 2 cm^{-1}. The last spectrum recorded after 24 h was used for secondary structure determination, representing the fully deuterated inactive state conformation (Fig. 3A). BetP activation was induced by replacing NaCl with 0.5 M KCl in the perfusing ^2H_2O-buffer [6,28] and spectra were recorded at 2 min time intervals for 2 h, averaging 128 scans for a spectral resolution of 2 cm^{-1}. Difference spectra were recorded by using spectra of the fully deuterated protein in the inactive state conditions as background. This step is referred to as the "first cycle of activation". 0.5 M NaCl was used again to induce the inactive state, in which the protein was equilibrated for 2 h and was activated again with 0.5 M KCl for the second time, which is referred to as the "second cycle of activation" within the text. In order to discriminate the effect of deuterium change from the structural changes upon activation, this cycle of buffer change was performed twice. The last spectrum recorded after the second cycle of activation was used for structure determination analysis, representing the fully deuterated active state conformation. In order to ensure the structural stability of the protein throughout the experiment, the temperature was set to 4 °C via a circulating water bath.

2.3. Processing of spectra

2.3.1. Side chain subtraction

Residual side chain subtraction, in principle, requires the exact knowledge of the protonation state of each side chain. However, only vibration modes of expected protonation states at pH 7.4 could be considered for subtraction, resulting in residual side chain absorbance due to protonated/deprotonated amino acids. In general, the C–C stretching mode of Tyr-signal at 1515 cm^{-1} can be exploited as an internal reference to scale the total side chain absorption with the calculated sum of side chain signals [29–31]. However, in the BetP spectra, subtraction of the Tyr-signal indicated the existence of protonated tyrosine residues, which, then, did not give a reliable spectral rationing factor. Therefore, the shoulder at 1583 cm^{-1} in the amide II region (Fig. 2B) originating from asymmetric stretching mode of deprotonated carboxyl groups of aspartate and glutamate residues and the symmetric stretching mode of $CN_3H_5^+$ from arginine was taken as the internal reference for side chain subtraction in BetP spectra [19]. Complete disappearance of this shoulder indicated successful subtraction of the side chain contribution (Fig. 2B). Subtraction of side chain contributions from the IR spectrum of the protein was performed according to the method documented previously [32–34]. Since BetP was equilibrated in ^2H_2O-buffer, the side chains in the hydrophilic region are in deuterated form but those in hydrophobic region are not affected by ^2H_2O-buffer. Therefore, the number of amino acids in the hydrophilic region and in hydrophobic region was counted from the crystal structure and their spectral contributions were subtracted separately from the BetP spectrum.

2.3.2. Curve fitting

The positions of minima in the second derivative profile of the spectrum were used to determine the number and position of the individual signals underlying the region between 1780 and 1490 cm^{-1}. This spectral window includes amide I and II regions as well as the C═O stretching modes originating from side chains. Fitting such a large region of the spectrum is definitely challenging; however, the sub-bands located in the border regions from amide I to amide II and from amide I to higher wavenumber regions are better determined. Generating a straight line between the two sides of Amide I for secondary structure analysis can also be applied for this purpose; however, great care should be taken in the analysis of the fit results, particularly at wavenumbers close to the end points of the region of interest. Although this method of generating a straight line also gives reliable information regarding the relative sub-band areas, and thus giving relative contribution of different secondary structure elements, the results do not always match with the crystallography data. Therefore fitting a larger area was preferred in this study. Potentially this method is more prone to user-oriented mistakes, in which one misidentified sub-band leads to a cascade of mistakes. In order to rule out the 'user' factor, the success of the curve-fit was determined by comparing the second derivative profile of the sample spectrum and the fit envelope, which is basically the sum of fitted sub-bands.

A built-in iterative macro in the software OPUS 4.2 (BRUKER Optics, Ettlingen, Germany) was used for curve-fitting routine. The number and position of sub-bands were entered to the software and the software did not allow their change during iterations. The software optimized band height, width and shape until a good match between the second derivative profiles were obtained while minimum root mean square (RMS) error was achieved.

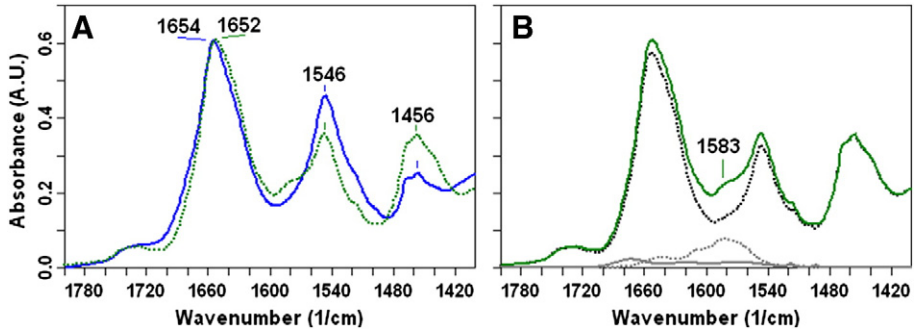

Fig. 2. (A) IR absorbance spectrum of detergent solubilized BetP in 0.1 M KP_i, 0.1% DDM, 0.5 M NaCl pH 7.4 (blue) and in deuterated buffer with 0.1 M KP_i, 0.1% DDM, 0.5 M NaCl p^2H 7.4 (dotted-green). (B) BetP in ^2H_2O-buffer before (green line) and after side chain subtraction (dotted-black). Side chain contributions of deuterated BetP located in the hydrophilic regions (grey) and those located in the hydrophobic region (dotted-grey) were calculated separately and subtracted from the raw spectrum. Disappearance of the shoulder at 1583 cm^{-1} was taken to be the internal control of complete side chain subtraction (dotted-black).

2.3.3. Deconvolution

Fourier Self Deconvolution was used to deconvolve the overlapped bands with a built-in macro in the software OPUS 4.2. A Lorentzian bandshape with 28 cm^{-1} bandwidth was used.

2.3.4. $^1H/^2H$ exchange

The protein spectra in ^1H_2O and ^2H_2O buffer were corrected using a built-in macro in the OPUS software [22]. In order to calculate the $^1H/^2H$ exchange rate of the protein, amide I and II bands were integrated from spectra. The amide II areas at both buffer conditions were compared by using integrated amide II/I ratio. The ratio was set to 0% for the sample spectrum in ^1H_2O buffer, so that a complete disappearance of the amide II band would correspond to 100% exchange with ^2H_2O.

3. Results

We performed FTIR spectroscopy experiments on detergent solubilized full length wild type BetP that was activated by addition of 500 mM K^+. The characteristic IR signals were analyzed and assigned to secondary structure elements. Subsequently, these assignments enabled us to interpret the difference spectra recorded with the ATR-FTIR perfusion microcell. In an infrared spectrum, the C═O stretching vibrational mode, originating from the protein backbone, gives rise to the amide I band (1700–1600 cm^{-1}) providing information on the peptide bonds of ordered structure elements, e.g. the secondary structure (Fig. 2A). The C–N stretching and N–H bending modes give rise to the amide II band (1600–1500 cm^{-1}) reflecting the quaternary structure and is used to monitor the amount of hydrophilic parts and the solvent accessibility of the protein. Side chains are seen in the 1750–1400 cm^{-1} region of the spectrum and allow the survey of protein-ligand/lipid interactions if proper assignment was applied (see below) [22,23]. Experiments were performed in ^2H_2O buffer in order to discriminate secondary structure elements and side chain contributions, since different molecular groups shift to different spectral regions during a change from ^1H_2O to ^2H_2O allowing for an unambiguous band assignment.

Proteins having mostly α-helical or β-plated sheet structure as the main folding motif differ in the amide I and II peak positions in the IR spectrum. The secondary structure composition of BetP yielded an amide I band positioned at 1654 cm^{-1} in H_2O-buffer and at 1652 cm^{-1} in ^2H_2O-buffer, while the amide II peak is observed at 1546 cm^{-1} in both conditions (Fig. 2A). Absorbance contributions from amino acid side chains were subtracted prior to further spectral analysis. Curve fitting of Amide I band revealed the underlying signals that originated from ordered structure elements (Fig. 3), which were distinguished under inactive (Fig. 3A, 0.5 M Na^+) and active (Fig. 3C, 0.5 M K^+) conditions. Most studies in literature use the RMS deviation of the fit result from the raw spectrum to validate the curve-fitting analysis [29,35,36], although, it is possible to have more than one fit solution with quite similar RMS values. Therefore we considered the second derivative profiles of the fit envelope in comparison to the original spectra as well (Fig. 3B and D).

The band located at 1655 cm^{-1} is attributed to the α-helical content [20,37], while the bands at 1634 and 1639 cm^{-1} are assigned to unordered structure, and/or loops in hydrophilic regions outside the membrane as well as solvated short helices and/or 3_{10} helices [20,38,39]. The peak at 1681 and 1674 cm^{-1} can be attributed to hydrogen bonded turns or closed loops buried in the hydrophobic region, located most likely in the membrane, thus unaffected from ^2H_2O-buffer. Inter-monomer contacts and/or intermolecular β-sheet structures give rise to the signals at 1623, 1629 and 1688 cm^{-1}. Residual side chain absorbance was observed at 1616 and 1605 cm^{-1}, resulting from protonated side chain states since normal modes were subtracted prior to curve-fitting analysis, particularly due to the protonated Tyr C–C stretching mode (Fig. 3). Therefore these signals were not considered for the secondary structure composition calculations presented in Table 1.

The relative proportion of each band with respect to the total amide I area is presented in Table 1. Since each sub-band represents an ordered structural element, relative proportion of each band gives the relative proportion of a specific secondary structure with respect to the complete protein. The secondary structure determination by FTIR differed from the distribution of structural elements observed in the crystal structures of BetP (pdb entry code 2WIT) (Fig. S1) [10]. Under inactive conditions, FTIR spectroscopy detected 21.5% in unordered elements, 3_{10} helices and/or short helices, while these contributed only 18% to the X-ray structure and might additionally be caused by stabilizing crystal contacts. The α-helical content was also found to be significantly higher with 71.5% as compared to 65% observed in the structure.

3.1. Secondary structure

We assume that a large fraction of the increased α-helical content with respect to the X-ray data is attributed to the 60 a.a.-long N-terminal domain. Well-diffracting crystals required truncation of the N-terminal domain by at least 29 residues [10], and thus, this part of BetP could not yet be resolved in X-ray studies (Fig. S1C). In total, the truncated residues together with the unresolved residues account very well for the 6% difference in the α-helical content. Indeed the N-terminal domain shows some propensity for a helical organization according to the secondary structure prediction using PSIPRED [40]. According to IR data, we suggest that at least half of the N-terminal domain might be in α-helical conformation.

Upon activation, we detected small number of re-arrangements in the secondary structure of BetP (Table 1). The total fraction of α-helical elements and of hydrophobic loops/turns decreases by

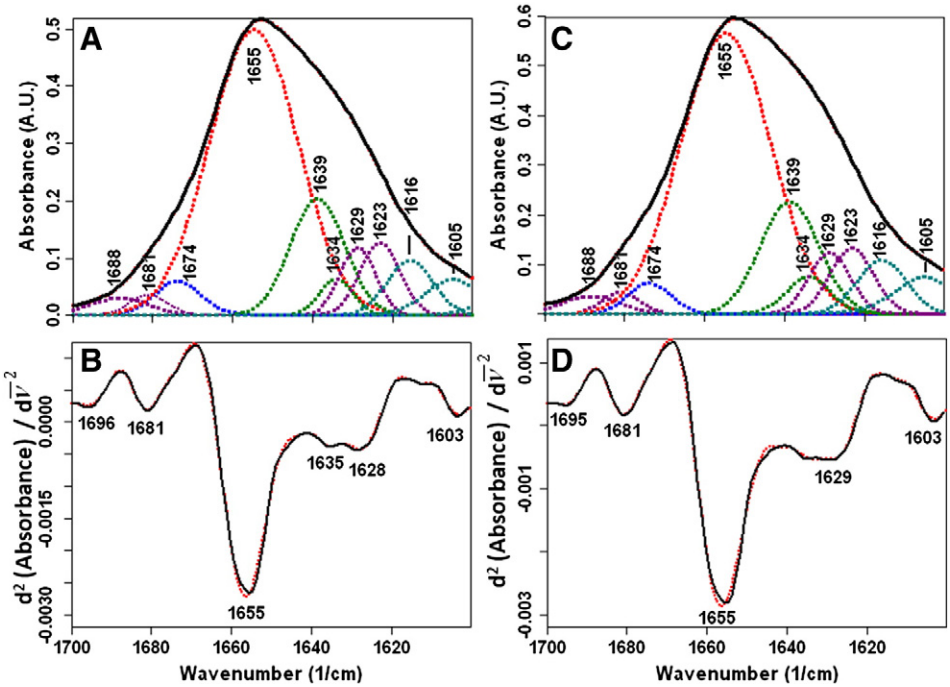

Fig. 3. Curve-fitting of IR spectra of deuterated BetP in inactive (A) and active (C) state. Activation is induced by adding 0.5 M KCl to the 0.1 M KP_i p^2H 7.4, 0.1% DDM buffer. Agreement between the second derivative profiles of the original spectrum (black line) and the sum of fitted curves (red dashed line) in inactive (B) and active state (D) is used for validation of the curve-fitting procedure. The root mean square (RMS) errors of the fits are 0.000174 and 0.000194 for the inactive and active state, respectively.

0.8% and 1%, respectively, under activation, while the amount of unordered elements, 3_{10} helices, short helices, and/or hydrophilic loops increases by 1.8%. These changes correspond to approx. 10–12 residues in BetP. Increasing and decreasing percentage fractions are consistent. Taken into account the satisfying fit RMS errors (see Fig. 2 legend) and the match between the raw spectrum and the fit envelope in their corresponding second derivative profiles (Fig. 3B & D), we are confident that these changes are significant. In overall, these changes indicate either a partial unfolding of helices or some helices becoming solvated upon activation.

3.2. K^+-effect on ionic networks

In order to investigate conformational changes of arginines, glutamates and aspartates during BetP activation, difference spectra of BetP have been recorded using ATR-FTIR perfusion system. Side chain subtraction was evidently not applied in these experiments. Activation of deuterated inactive BetP was induced by adding 0.5 M KCl to the ^2H_2O-buffer and the difference was recorded with respect to the inactive state (Fig. 4, black spectrum). To avoid the structural alterations due to electrostatic shielding and unspecific ionic strength effects induced by the addition of high concentration of salt, inactivation of BetP was induced by replacing KCl with NaCl, thus keeping the salt concentration constant at all time. Since the experiment was performed in ^2H_2O-buffer, the first cycle of activation includes spectral signatures due to both activation and further deuteration; i.e. protein regions newly accessible by ^2H_2O upon activation. To distinguish between the two effects, a second cycle of activation was performed, where the recorded spectra consequently reflected only changes due to activation (Fig. 4, red spectrum).

All difference peaks were very broad suggesting that they comprise overlapping signals. Deconvolution and derivative formation are the most commonly used spectral enhancement methods for overlapped signals in IR spectroscopy. The deconvoluted and the reciprocal of the second derivative profile of difference spectra are shown in Fig. 5A and B, respectively, for better distinction of the underlying signals. Since deconvolution enhances the spectral noise as well, the second derivative profile was also used in the analysis and

Table 1
Secondary structure composition of BetP in active and inactive states as deduced from IR spectroscopy in comparison to X-ray data. The band area of each signal is proportioned to the total Amide I area for the given percentage fractions.

IR signal position	Assigned secondary structure	BetP — inactive state (%)	Approximate number of a.a. involved[a]	BetP — active state (%)	Approximate number of a.a. involved[a]	X-ray data[b] (%)
1634 cm^{-1} 1639 cm^{-1}	Unordered; 3_{10} helix; short helix; open loops	21.5	128	23.3	139	18[c]
1655 cm^{-1}	α-helix	71.5	425	70.7	421	65
1674 cm^{-1} 1681 cm^{-1}	loops and turns	4.9	29	3.7	22	7
		2.1	13	2.3	14	
1623 cm^{-1}	Inter-monomer contacts and/or intermolecular β-sheet	6.9	75	6.8	76	4 [14]
1629 cm^{-1}		5.8		6.0		
1688 cm^{-1}		2.5		2.5		

[a] The number of amino acids giving rise to the indicated band in each row was calculated by forming the ratio of the band area to the total amide I area, which corresponds to 595 a.a.
[b] PDB entry: 2WIT. The published secondary structure percentage is calculated with respect to 566 residues (29 a.a. truncated from N-terminus). For the given fractions above, the percentages were recalculated with respect to 595 residues in order to compare with IR spectral data.
[c] In the published structure 84 residues (14%) are unassigned, corresponding to unordered structure and loops; 14 residues (2%) are assigned to 3_{10} helices. The solvated short helix EL2, having 9 residues (1.5%), is also included in the given percentage fraction.

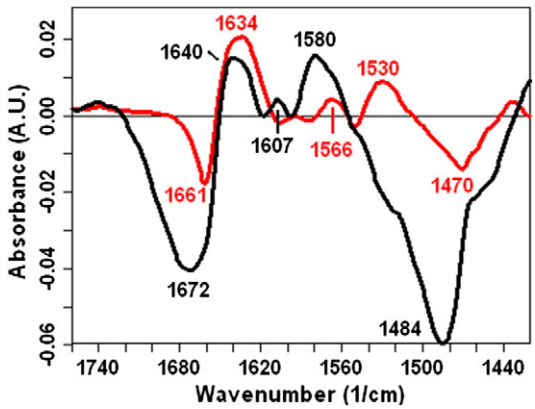

Fig. 4. IR difference spectra of BetP showing the first cycle (black) and the second cycle (red) of activation in ^2H_2O-buffer (see text). Difference spectra are recorded taking the inactive state as reference, thus positive peaks are associated with the active state and the negative peaks are associated with the inactive state of the protein. The first cycle shows conformational changes with activation and the backbone regions/side chains of the protein newly exposed to ^2H_2O-buffer. The second cycle shows only the conformational changes due to activation of the protein.

only the peaks that appear in both profiles were taken into consideration. A list of all the peaks shown in Fig. 5 is given in Table S1.

Deconvolution revealed a negative peak at 1677 cm^{-1}, which is resolved into two negative peaks at 1681 and 1670 cm^{-1} by the second derivative (Fig. 5B) in the first cycle of activation. Although both peaks can be assigned to loops and turns, 1670 cm^{-1} is more likely to represent Arg residues based on the positive 1608 cm^{-1} signal. The antisymmetric stretching mode of $CN_3H_5^+$ group in Arg has been previously reported to be located at ~1672 cm^{-1} in H_2O buffer; and thus, the positive peak at 1608 cm^{-1} is assigned to solvent exposed Arg residues in ^2H_2O buffer [32,33]. These signals argue that there are Arg residues shielded from buffer solution in inactive state, which are deuterated only upon activation. Out of 25 arginines in BetP, most are located in the hydrophilic region and among them, half are located in the C-terminal domain and in the cytoplasmic loops 2 and 8. The FTIR difference spectra propose a change in Arg residue solvent accessibility upon K^+ induced activation, suggesting a modification in the interactions of the C-terminal domain.

The changes in the spectral region 1800 and 1700 cm^{-1} are due to changes in the H-bonding properties of carboxylic groups of Asp and Glu (Fig. 5B). Based on the width of the signal(s), it is evident that several amino acids are involved in the activation of BetP. Deconvolution of this large band reveals six underlying signals located at 1739 (+), 1733(−), 1725(+), 1717(−), 1710(+) and 1697 cm^{-1} (−). These series of positive and negative signals indicate a change in the H-bonding properties of Asp and Glu upon activation of BetP [23,41,42]. The asymmetric stretching vibrational modes of the deprotonated carboxylic groups are located at 1584, 1567 cm^{-1} [32]. In deconvoluted difference spectrum of the first cycle of activation (Fig. 5A-black line) two positive signals are located in the amide II region at 1582 and 1566 cm^{-1}. These signals are located at comparable positions with published data. Positive signals at these positions suggest that upon activation, some of the Asp and Glu are deprotonated and some are protonated based on the positive signals in 1750–1700 cm^{-1} region. The change in the protonation states of Arg, Asp and Glu might suggest salt bridge formations that are altered upon K^+ induced activation. This is also in agreement with the interactions between Arg–Asp and Arg–Glu observed in the X-ray structure (Fig. 1C, inset) [10,12].

In order to understand the relative amount of interchange between different peaks in the 1700–1750 cm^{-1} region, curve-fitting analysis has been applied to the absorbance spectra in ^2H_2O buffer, in active and inactive conditions of the protein (Fig. 6). The carboxylic groups of protonated aspartic and glutamic acid residues gave rise to a broad peak centered at ~1735 cm^{-1}, extending from 1700 to 1770 cm^{-1}. The curve-fitting analysis revealed three peaks in this region of the IR spectrum (Fig. 6). The position of the peaks remained unaltered under inactive and active conditions; however, the percentage fraction of each sub-band changed by 2–5%, corresponding roughly to 12–30 aa. Based on the positions of the three underlying peaks, it is possible to classify the hydrogen bond protomer–protomer interactions involving Asp and Glu residues in three groups as weak, medium and strong (Table 2). The majority of the protonated carboxyl groups interact moderately as deduced from the relative fraction of the 1729 cm^{-1} band. By switching from inactive to active

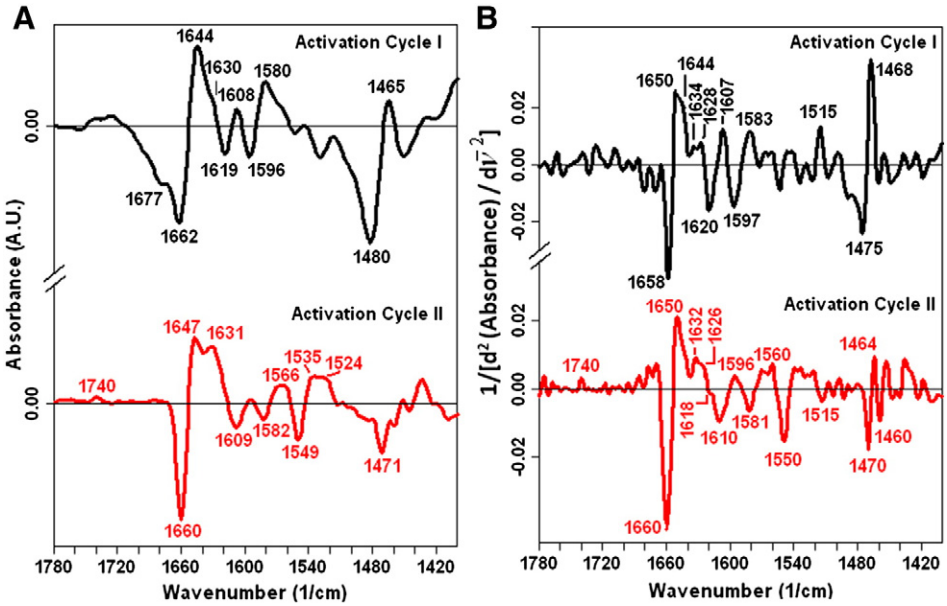

Fig. 5. Deconvoluted difference spectra (A) and the reciprocal of the second derivative profiles (B) of the first (black) and second (red) cycle of activation of BetP in ^2H_2O-buffer. Deconvolution is performed with a Lorentzian bandshape with 28 cm^{-1} bandwidth. In B, the reciprocal of the second derivative profiles is given for easier visual comparison with deconvoluted spectra.

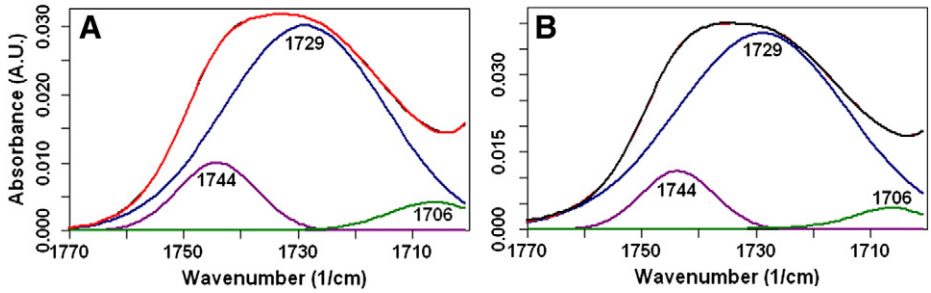

Fig. 6. Curve-fitting analysis results of the C═O region (1770–1700 cm^{-1}) of the IR spectrum of BetP in the inactive (A) and the active (B) state. This region represents the hydrogen bonded — C═O groups originating from aspartic or glutamic acid.

state, the contribution of the signals at 1706 and 1744 cm^{-1} decreased by 2% and 3%, respectively, while we observed an increase at 1729 cm^{-1} by 5%. From the results of curve-fitting analysis, we propose that upon BetP activation the interaction partners within the ionic interaction network are changing.

Two cation-pi interactions (Trp141-ARg390 and Trp431-Arg167) were suggested to play important roles in the stabilization of the regulatory ionic networks (Fig. 1C, insets). We tentatively assign the interchange between 1475/1470 cm^{-1} and 1468/1464 cm^{-1} seen in the 1st/2nd cycle of activation in Fig. 5B to tryptophan residues undergoing reorientations upon K^+-activation [43]. This interchange between the two signal positions is common for both cycles; therefore we assume that reorientations of tryptophan residues are correlated with activation but not with further deuteration.

3.3. Protomer–protomer interactions

In the region of the amide I band, curve-fitting analysis revealed a broad high frequency signal at 1688, and two low frequency signals at 1629 and 1623 cm^{-1} (Fig. 3A & C). Assuming that the broad high frequency component results from two overlapping component signals, we assign these signals to intra- or intermolecular contacts as their signals are often found in pairs; one at ~1630 cm^{-1} and the other at ~1685 cm^{-1} [26,44,45]. In this region bands at 1688, 1629 and 1623 cm^{-1} reflect either protomer–protomer contacts within an oligomeric assembly or contacts among ordered structures within a monomer, which is termed as "intermolecular β-sheet" [46]. Since side chain contributions were subtracted prior to curve-fitting analysis and there is no β-sheet structure in BetP, intermolecular β-sheet is the only candidate for the assignment of these signals. To detect an intermolecular β -sheet signal, two secondary structure segments should approach one another without the interference of lipids or detergent similar to what can be observed as intermolecular interaction in e.g. a β-barrel. In BetP, close interactions among TM helices occur along with the 4-TM helix bundle and the scaffold domain (Fig. 1A). Therefore a split in frequency (1623 and 1629 cm^{-1}) would reflect differences in interaction properties and/or strengths either within the trimeric transporter structure or within an individual protomer [36]. Higher wavenumbers represent weaker interaction, whereas a shift to lower wavenumbers accounts for stronger interaction. A very likely interpretation is that appearance of multiple bands in the context of protomer–protomer contacts indicates different trimeric assemblies, e.g. populations of trimers that might exhibit differences in the contact distance along the trimeric interface (Fig. 1C). While in the context of intermolecular interactions within an individual protomer, we have to assume differences in transporter conformations. The total band area of the split signals with respect to the total amide I band area was only slightly influenced due to K^+ activation (Table 1), i.e., the total number of interacting residues was unaltered between the active and inactive state of BetP. However, the contribution of the band at 1629 cm^{-1} is increased while the contribution of the band at 1623 cm^{-1} is decreased upon activation, indicating that the interactions among the contacts are stronger when the protein is in inactive state (Table 1).

Difference spectra recorded with activation shows a positive peak at 1628 cm^{-1} and a negative peak at 1620 cm^{-1} (Fig. 5B), indicating a change in the properties of interactions among ordered structure elements. Upon activation, intermolecular interactions get weaker as compared to the inactive state of BetP, as the curve-fitting analysis has suggested.

Table 2
C═O modes of protonated Asp and Glu give rise to a composite band in the wavenumber region 1700–1760 cm^{-1}. According to the nature of the interaction between the H-bond donor and acceptor, the bands are denoted as strong, medium and weak. Sub-band positions were determined from the second derivative of the IR spectrum and curve-fitting analysis was performed on deuterated BetP in active and inactive states. The percentage fraction of a fitted band was calculated by forming the ratio with the total band area.

IR signal position	H-bonding	Assignment	BetP-inactive (%)	BetP-active (%)
1706 cm^{-1}	Strong	Protonated Asp/Glu	7.0	5.2
1729 cm^{-1}	Medium		79.9	84.6
1744 cm^{-1}	Weak		13.1	10.2

3.4. Backbone accessibility during activation

When proteins are equilibrated in ^2H_2O-buffer, N–H interactions in the backbone become deuterated if accessible to ^2H_2O-buffer. The N–^{2}H mode has a vibration frequency ~100 cm^{-1} lower than that of the N–H mode, and thus, can be easily differentiated in the IR spectrum. Amide II band arises from N–H bending and C–N stretching modes. When the buffer is switched to ^2H_2O, amide II band is deprived of N–H modes of amides that are accessible by buffer solution. Thus, comparing the initial and final band areas of amide II band is an indicator of how much of the protein is exposed to a hydrophilic environment, allowing the estimation of protein backbone accessibility to buffer solution. This calculation yields that 55% of the protein backbone is accessible to ^2H_2O after 24 h of equilibration under inactivated conditions (Fig. 2A-blue spectrum and Fig. 2B-black spectrum). In the presence of excess K^+ in the buffer solution, further exchange to ^2H_2O was observed accounting for about 11%, i.e. 65 additional residues. Percentage fractions depend strongly on how the baseline is drawn before the integration. In this study, a baseline drawn from the left edge of amide II was used. Therefore deducing the number of amino acids in hydrophilic regions requires careful calculation; however comparison of different states at different times is quite reliable as long as the integration method applied is the same. Consequently, activation of BetP causes residues that were previously inaccessible to buffer to be accessible. Judged from the quite high number of additional residues, we assume that this concerns mostly the residues buried within the transmembrane part of BetP, probably together with a few hydrophilic residues that are part of rigid helical segments.

3.5. Helix solvation and conformation

The most dramatic change in the deconvoluted spectrum of the first cycle of activation was the decrease of the band at 1662 cm^{-1} and the concomitant increase at 1644 cm^{-1} (Fig. 5A). Furthermore, in the corresponding second derivative profile (Fig. 5B) the positive band is seen to be well resolved into three components; 1650, 1644, and 1634 cm^{-1}. It has been previously reported that long/solvated helices absorb at lower wavenumbers compared to shorter/membrane-located helices [36,39,47,48]. It is evident from the shift of the band at 1658 cm^{-1} to 1650 cm^{-1} (Fig. 5B) that some parts of long helices make additional hydrogen bonds with the buffer solution upon activation, thus shifting to lower wavenumbers. In the second cycle of activation (Fig. 5B) a similar shift was also observed, where the band at 1660 cm^{-1} shifts down to 1647/1650 cm^{-1}. Based on the fact that this spectral shift was observed every time the protein is activated argues that hydration of helices is not due to $^{1}H/^{2}H$ exchange but due to BetP activation. Helices in hydrophobic region are also suggested to absorb at higher wavenumbers compared to solvent-exposed helices [48]. The interchange between the two types of helices in BetP, in switching from inactive to active state, does not change the overall peak position of amide I (data not shown). Therefore it is possible that the orientation of helices changes with respect to the membrane normal by solvation upon activation as it was previously reported for the melibiose transporter MelB [38].

4. Discussion

4.1. Regulation and trimeric state

Accumulation of compatible solutes by osmotically controlled uptake systems is a major bacterial stress response strategy to ensure a physiologically acceptable level of cellular hydration and turgor at high osmolarity [1]. The betaine transporter BetP from *C. glutamicum*, which functions both as an osmosensor and osmoregulator, became a paradigm for regulated transport since its crystal structure has been solved [10]. Based on the structure and the wealth of biochemical data on BetP regulation, a first correlation between the stress sensing and regulation of transport activity has been drawn [10,14]. However, a crystal structure represents a molecular snapshot depicting just one population of a whole ensemble of different conformational states. In addition, this conformational state might be restricted in functional and/or dynamical interactions by crystal contacts. Therefore, we recognize a gap between our molecular static knowledge and the functional and biochemical data, especially when we wish to describe the dynamic behavior of BetP during stress-induced activation.

Transport regulation in BetP is crucially linked to the trimeric state [14] and supposable other trimeric transporters, e.g. the glutamate transporter, might exploit their oligomeric state for functional purposes, too [49]. The monomeric form of BetP as well as the C-terminal truncated form of trimeric BetP is not activity regulated [12]. Mutagenesis and computational studies revealed that the trimeric state of BetP provides the platform for at least two regulatory ionic interactions. They are part of the protomer–protomer contacts although they are not dominantly contributing to trimer stabilization [12]. The most obvious consequence of this interaction in the context of regulation of transport would be a restriction of the mobility of TM3, which undergoes a major conformational change during the transport cycle [11]. Assuming that these networks have a restrictive effect on BetP under inactivating conditions they should subsequently be loosened or released during activation.

The assumption of a dynamical intra-trimeric ionic network, which changes upon activation, was recently discussed based on EPR studies on BetP [16] indicating that the trimeric interface at the cytoplasmic side is affected by K^{+}-activation. Here, we applied FTIR spectroscopy to tackle the question on conformational changes in the secondary structure of BetP upon K^{+}-induced activation. FTIR allows the investigation of secondary structure elements without constraints of crystal contacts addressing even very subtle changes in side chain conformation during the dynamic process of activation. FTIR difference spectroscopy was used successfully in studies on membrane proteins [38,50,51], e.g. to investigate substrate-induced conformational changes in the melibiose carrier MelB from *E. coli* showing the coupling between the ion- and sugar-binding sites [52].

The way we analyzed our FTIR spectra allowed for an assignment of the individual signals to changes in secondary structure, protomer–protomer interactions and backbone accessibility. Moreover, ionic interactions could be monitored quantitatively for individual side chains. FTIR provides very detailed biophysical information of partial elements in a protein; however, in small 'packages' that have to be combined like puzzle pieces based on structural and the detailed biochemical knowledge to reveal the entire picture of a molecular mechanism.

Neither secondary structure elements nor the protomer–protomer interactions changed dramatically upon activation. FTIR data reveal that regulation involves only subtle changes of the secondary structure of about 1–2%. At the same time, the total amount of residues involved in protomer–protomer interactions within the trimer remains unaltered, but FTIR suggests a change in the nature of interaction. This is an important finding, indicating that the intraprotomeric ionic network is maintained although individual residues might switch interaction partners upon activation. Difference spectra of K^{+}-induced BetP activation showed spectral signatures indicating salt bridges formation between Arg and Asp/Glu, which is in very good agreement with the regulatory interaction networks already described previously [10]. The changes in protonation states of Asp and Glu upon activation/deactivation correlate well with the interactions between Arg–Asp and Arg–Glu observed in the X-ray structure [10,12].

FTIR might also contribute a new detail on BetP's conformationally asymmetric protomer architecture [11]. Two populations of BetP trimers adopting either different protomer–protomer interaction strength or protomer conformation distributions were detected. The populations differ with respect to side chain interaction distances characterized by either strong or weak interactions involving ~30 residues. It is tempting to speculate that we observe here the consequences of the asymmetric trimer architecture [53], which in the absence of crystal contacts allow one trimer to adopt a dynamic distribution of conformational states. Our crystallographic data have indicated that during alternating access cycle BetP performs a transition between outward-facing and inward-facing state via an intermediate closed state [12]. This closed state is significantly different in main chain arrangement from outward- and inward-facing state, e.g. there is an increase in secondary structure interactions to occlude cytoplasmic and periplasmic pathways [12]. In this context, we assume that the split signals might reflect both a flexible trimer interface and a distribution of protomers that adopt a closed state.

As the population is shifted toward weaker interactions upon K^{+}-induced activation, we suggest that the closed state is less populated during activation. Simultaneously the trimeric interface might adopt a more flexible architecture.

Moreover, our FTIR data point toward significant contributions of charged residues suggesting that we predominately detect the ionic interaction of terminal domains with cytoplasmic loops [10]. The amount of interacting residues indicated by FTIR is three times higher than ionic interaction sites identified in the structures [10]. However, we have to consider that the C-terminal domains are not entirely resolved in BetP X-ray structures. Very recent EPR studies on BetP propose that K^{+}-activation triggers changes at the trimeric interface around Tyr550 rather than a rigid-body reorientation of the entire C-terminal domain [16]. Considering also putative interaction sites in the range of 4–5 Å and assuming a similar architecture of the two C-terminal domains (Fig. 7) we identified multiple interaction modes of the C-terminal domains with other C-terminal domains

with each other, with loop4 and with loop6. Peptide array analysis as well as a functional competition assay in proteoliposomes clearly shows that residues in loop4 and loop6 strongly interact with the C-terminal domain [13]. In addition, we identified two lysines, Lys214 in loop4 and Lys300 in loop6, which are potential interaction partners for the α-helical C-terminal domain (Fig. 7). ATR-FTIR data revealed unambiguously a strong effect on the amount of solvent exposed arginines. Out of 25 arginines in BetP, half of them are located in the C-terminal domain and a cluster of 8 arginines is located at the very end of the C-terminal domain (R574-R595). This domain shows low helical propensity and is not resolved in the structure. The FTIR difference spectra propose an increase of accessibility upon K^+ induced activation, which would point toward an effect on unfolding of exactly this region.

4.2. Folding and unfolding during activation

We assume that the decrease in helical content in secondary structure is attributed to the C-terminal domain that is the key player in transport regulation. FTIR results show strong evidence for a regulated unfolding event of the osmosensing C-terminal domain that is in agreement with the molecular switch activation model [13] of BetP. This model suggests a conformational change of the C-terminal domain, switching interactions between cytoplasmic loops and negatively charged lipids from the surrounding membrane [13].

A detailed site-directed mutagenesis analysis on the impact of charged residues within the α-helical C-terminal domain on the regulatory properties of BetP suggests that the majority of charged residues in this domain are involved in regulation [13]. In fact, most of the residues we identified based on the FTIR results as candidates for protomer–protomer interaction are crucial for regulation in *E. coli* membranes (Fig. 7, residues colored in orange). For their functional availability, the α-helical fold of the C-terminal domain seems to be required. Interestingly, only a few residues in the C-terminal domain were sensitive to single point mutation of charged residues to proline (Fig. 6, colored in yellow) with respect to deregulation in negatively charged membranes. Unfolding of the C-terminal domain might occur at the last 20 amino acids. These residues are not important for regulation directly [13], but their interactions with either lipids or cytoplasmic loops, e.g. loop4 or loop6 (Fig. 7) have an impact on the fold of the mid-region of the C-terminal domain. Based on the hypothesis that additional interaction partners were proposed from peptide array analysis and competition studies [13], the possible interaction of the C-terminal with the N-terminal domain comes into the center of attention.

4.3. Structure of the N-terminal domain

In this study, a detailed analysis of the amide I band region (1700–1600 cm^{-1}) provided spectral evidence that the α-helical content of BetP is significantly higher than anticipated from the X-ray data, suggesting that indeed the N-terminal domain has at least partial α-helical order (Table 1). There is low propensity for two α-helical structures (P17-L30 and A43-L49) but most likely helical folding requires further stabilizing interactions with other parts of BetP. Hypothesizing that the N-terminal domain interacts with the C-terminal domain of a neighboring protomer, e.g. the C-terminal domain of protomer A with the N-terminal domain of protomer C (Fig. 7). The N-terminal domain might require an ordered helical fold to position the two charged clusters (E24E25 and E44E45E46) in an appropriate orientation. The second cluster was identified in the peptide array analysis to interact specifically with the C-terminal domain [13]. In addition, AFM data revealed an intermolecular interaction site close to the triple-glutamate cluster 44EEE46 that is reacting to activating K^+ concentrations [15]. Based on the FTIR data we speculate that the N-terminal helical segments might fold to provide a stabilizing interaction interface in the helical segment 2 (Fig. 7), which in turn affect the helical fold of the C-terminal domain in a given orientation and most importantly in competition with the negatively charged lipids. The consequence of such an alternative (yet fictive) helical

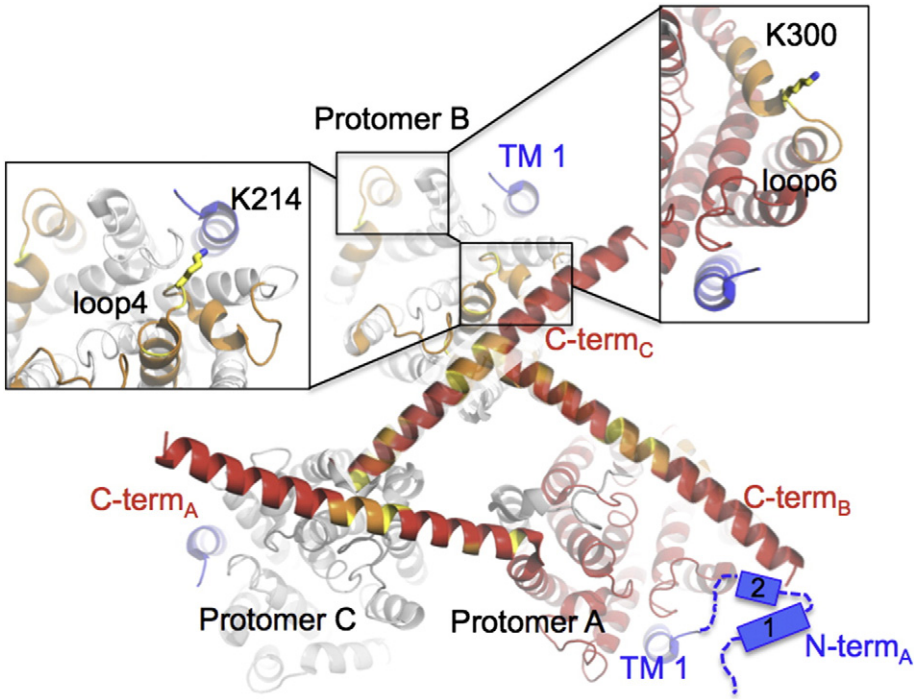

Fig. 7. Top view on the cytoplasmic side of the BetP trimer. The C-terminal domain of protomer A is overlaid on the domains of protomer B and protomer C to demonstrate a possible orientation and interaction with the perimeter of the corresponding adjacent protomer. Positions of charged residues within a helical ordered C-terminal domain, which affect regulatory properties in *E. coli* membranes are colored in orange and those in *C. glutamicum* membranes are colored in yellow. Unfolding of the C-terminal domain might occur at the last 20 amino acids, which are colored in red. The N-terminal domain and TM1 is colored in blue.

orientation, as it is depicted for the C-terminal domain of protomer B (Fig. 7), would be that the cytoplasmic interaction network is restricting the movement of TM3 by an altered interaction with loop2, rendering the substrate pathway into a more accessible state, which is exactly what FTIR solvent accessibility studies of the backbone and on helix solvation are indicating.

4.4. Terminal interactions render substrate-binding sites more accessible

BetP has an α-helical content of ~70% and we cannot rule out that small stretches of about 3–4 residues can unfold within a helix. In fact, BetP comprises a glycine and proline-rich belt along the pseudo-twofold axis running in the middle of the membrane, which relates both inverted structural repeat domains [10]. Certainly, this might provide a higher flexibility of the midsection of the twelve TM helices. In TM3, which exhibits a glycine rich stretch halfway across the membrane, flexibility is definitely an important element to facilitate both betaine and sodium binding [11]. Our results might provide some evidence that activation alters the hydrophobic core of BetP. The short, less tilted and/or membrane-buried helices (type I-helix) become solvated and/or tilted (type II-helix) upon K^+-induced activation. This result is further supported by the results of $^1H/^2H$ exchange. In fact, activation causes more protein backbone regions to be exposed to buffer solution. In the presence of excess K^+ in the buffer solution, about 11%, i.e. 65 additional residues become more accessible to buffer. AFM measurements have recently shown that under activating conditions conformational changes at the periplasmic side result in the formation of a second binding site [15], which would be in agreement with reorientations of tryptophan residues detected by FTIR. Judging from the reasonable high number of additional residues we assume that this concerns not only membrane-buried parts, but also some of the hydrophilic residues. BetP comprise a hydrophilic short helix in the periplasmic loop9 and the 3_{10} helix in the intracellular loop4. Both elements are structurally conserved in other LeuT-fold transporters [10]. Very recently it was proposed that in the corresponding loop9 of LeuT, the two short hydrophilic helices are critically involved in conformational changes to open and close the periplasmic substrate pathway [54]. We assume that the increased number of buffer accessible residues monitored by FTIR reflect conformational changes in both loops. The same holds for orientation changes in the C-terminal domains as a consequence of the putative partner switching mechanism, which might even open the central cavity of the trimer to some extent.

The proposed folding/unfolding of C-terminal domain and a possible interaction with the membrane surface will be the subject of future studies by FTIR spectroscopy, which has proven to be a powerful method simultaneously analyzing lipid–protein interactions [19,23,45].

Supplementary data to this article can be found online at http://dx.doi.org/10.1016/j.bbamem.2013.01.004.

Acknowledgements

Camilio Perez is gratefully acknowledged for helpful discussions about the BetP structure. We thank Caroline Koshy and Reinhard Krämer for careful reading and valuable comments. We thank Prof. Dr. Erik Goormaghtigh from Université Libre de Bruxelles, Belgium, for generously providing us with the software Kinetics for side chain subtraction.

References

[1] M. Farwick, R.M. Siewe, R. Kramer, Glycine betaine uptake after hyperosmotic shift in *Corynebacterium glutamicum*, J. Bacteriol. 177 (1995) 4690–4695.
[2] S. Morbach, R. Kramer, Impact of transport processes in the osmotic response of *Corynebacterium glutamicum*, J. Biotechnol. 104 (2003) 69–75.
[3] H. Peter, B. Weil, A. Burkovski, R. Kramer, S. Morbach, *Corynebacterium glutamicum* is equipped with four secondary carriers for compatible solutes: identification, sequencing, and characterization of the proline/ectoine uptake system, ProP, and the ectoine/proline/glycine betaine carrier, EctP, J. Bacteriol. 180 (1998) 6005–6012.
[4] R. Rubenhagen, H. Ronsch, H. Jung, R. Kramer, S. Morbach, Osmosensor and osmoregulator properties of the betaine carrier BetP from *Corynebacterium glutamicum* in proteoliposomes, J. Biol. Chem. 275 (2000) 735–741.
[5] H. Peter, A. Burkovski, R. Kramer, Osmo-sensing by N- and C-terminal extensions of the glycine betaine uptake system BetP of *Corynebacterium glutamicum*, J. Biol. Chem. 273 (1998) 2567–2574.
[6] R. Rubenhagen, S. Morbach, R. Kramer, The osmoreactive betaine carrier BetP from *Corynebacterium glutamicum* is a sensor for cytoplasmic K+, EMBO J. 20 (2001) 5412–5420.
[7] D. Schiller, R. Rubenhagen, R. Kramer, S. Morbach, The C-terminal domain of the betaine carrier BetP of *Corynebacterium glutamicum* is directly involved in sensing K+ as an osmotic stimulus, Biochemistry 43 (2004) 5583–5591.
[8] D. Schiller, V. Ott, R. Kramer, S. Morbach, Influence of membrane composition on osmosensing by the betaine carrier BetP from *Corynebacterium glutamicum*, J. Biol. Chem. 281 (2006) 7737–7746.
[9] T. van der Heide, B. Poolman, Osmoregulated ABC-transport system of *Lactococcus lactis* senses water stress via changes in the physical state of the membrane, Proc. Natl. Acad. Sci. U. S. A. 97 (2000) 7102–7106.
[10] S. Ressl, A.C. Terwisscha van Scheltinga, C. Vonrhein, V. Ott, C. Ziegler, Molecular basis of transport and regulation in the Na(+)/betaine symporter BetP, Nature 458 (2009) 47–52.
[11] C. Perez, C. Koshy, O. Yildiz, C. Ziegler, Alternating-access mechanism in conformationally asymmetric trimers of the betaine transporter BetP, Nature 490 (2012) 126–130.
[12] R.M. Gartner, C. Perez, C. Koshy, C. Ziegler, Role of bundle helices in a regulatory crosstalk in the trimeric betaine transporter BetP, J. Mol. Biol. 414 (2011) 327–336.
[13] V. Ott, J. Koch, K. Spate, S. Morbach, R. Kramer, Regulatory properties and interaction of the C- and N-terminal domains of BetP, an osmoregulated betaine transporter from *Corynebacterium glutamicum*, Biochemistry 47 (2008) 12208–12218.
[14] C. Perez, K. Khafizov, L.R. Forrest, R. Kramer, C. Ziegler, The role of trimerization in the osmoregulated betaine transporter BetP, EMBO Rep. 12 (2011) 804–810.
[15] L. Ge, C. Perez, I. Waclawska, C. Ziegler, D.J. Muller, Locating an extracellular K^+-dependent interaction site that modulates betaine-binding of the Na^+-coupled betaine symporter BetP, Proc. Natl. Acad. Sci. U. S. A. 108 (2011) E890–E898.
[16] S.C. Nicklisch, D. Wunnicke, I.V. Borovykh, S. Morbach, J.P. Klare, H.J. Steinhoff, R. Kramer, Conformational changes of the betaine transporter BetP from *Corynebacterium glutamicum* studied by pulse EPR spectroscopy, Biochim. Biophys. Acta 1818 (2012) 359–366.
[17] E. Dzafic, O. Klein, P. Goswami, W. Kuhlbrandt, W. Mantele, Infrared spectroscopic study of the structural and functional properties of the Na^+/H_+ antiporter MjNhaP1 from *Methanococcus jannaschii*, Biochim. Biophys. Acta 1787 (2009) 730–737.
[18] A. Barth, F. von Germar, W. Kreutz, W. Mantele, Time-resolved infrared spectroscopy of the Ca^{2+}-ATPase. The enzyme at work, J. Biol. Chem. 271 (1996) 30637–30646.
[19] E. Goormaghtigh, V. Raussens, J.M. Ruysschaert, Attenuated total reflection infrared spectroscopy of proteins and lipids in biological membranes, Biochim. Biophys. Acta 1422 (1999) 105–185.
[20] J.L. Arrondo, F.M. Goni, Structure and dynamics of membrane proteins as studied by infrared spectroscopy, Prog. Biophys. Mol. Biol. 72 (1999) 367–405.
[21] H. Fabian, W. Mäntele, Infrared Spectroscopy of Proteins, John WIley & Sons Ltd., Chichester, 2002.
[22] E. Dzafic, O. Klein, E. Screpanti, C. Hunte, W. Mantele, Flexibility and dynamics of NhaA Na(+)/H(+)-antiporter of *Escherichia coli* studied by Fourier transform infrared spectroscopy, Spectrochim. Acta A Mol. Biomol. Spectrosc. 72 (2009) 102–109.
[23] F. Korkmaz, S. Koster, O. Yildiz, W. Mantele, The role of lipids for the functional integrity of porin: an FTIR study using lipid and protein reporter groups, Biochemistry 47 (2008) 12126–12134.
[24] M. Beck, F. Siebert, T.P. Sakmar, Evidence for the specific interaction of a lipid molecule with rhodopsin which is altered in the transition to the active state metarhodopsin II, FEBS Lett. 436 (1998) 304–308.
[25] S. Sukumaran, K. Hauser, E. Maier, R. Benz, W. Mantele, Tracking the unfolding and refolding pathways of outer membrane protein porin from *Paracoccus denitrificans*, Biochemistry 45 (2006) 3972–3980.
[26] F. Korkmaz-Ozkan, S. Koster, W. Kuhlbrandt, W. Mantele, O. Yildiz, Correlation between the OmpG secondary structure and its pH-dependent alterations monitored by FTIR, J. Mol. Biol. 401 (2010) 56–67.
[27] S.G. Grant, J. Jessee, F.R. Bloom, D. Hanahan, Differential plasmid rescue from transgenic mouse DNAs into *Escherichia coli* methylation-restriction mutants, Proc. Natl. Acad. Sci. U. S. A. 87 (1990) 4645–4649.
[28] R. Kramer, S. Morbach, BetP of *Corynebacterium glutamicum*, a transporter with three different functions: betaine transport, osmosensing, and osmoregulation, Biochim. Biophys. Acta 1658 (2004) 31–36.
[29] J. Guldenhaupt, Y. Adiguzel, J. Kuhlmann, H. Waldmann, C. Kotting, K. Gerwert, Secondary structure of lipidated Ras bound to a lipid bilayer, FEBS J. 275 (2008) 5910–5918.
[30] C. Vigano, M. Smeyers, V. Raussens, F. Scheirlinckx, J.M. Ruysschaert, E. Goormaghtigh, Hydrogen–deuterium exchange in membrane proteins monitored by IR spectroscopy: a new tool to resolve protein structure and dynamics, Biopolymers 74 (2004) 19–26.
[31] H.H. de Jongh, E. Goormaghtigh, J.M. Ruysschaert, Monitoring structural stability of trypsin inhibitor at the submolecular level by amide-proton exchange using Fourier transform infrared spectroscopy: a test case for more general application, Biochemistry 36 (1997) 13593–13602.

[32] Y.N. Chirgadze, O.V. Fedorov, N.P. Trushina, Estimation of amino acid residue side-chain absorption in the infrared spectra of protein solutions in heavy water, Biopolymers 14 (1975) 679–694.
[33] S.Y. Venyaminov, N.N. Kalnin, Quantitative IR spectrophotometry of peptide compounds in water (H_2O) solutions.1. Spectral parameters of amino-acid residue absorption-bands, Biopolymers 30 (1990) 1243–1257.
[34] E. Goormaghtigh, V. Cabiaux, J.M. Ruysschaert, Determination of soluble and membrane protein structure by Fourier transform infrared spectroscopy. II. Experimental aspects, side chain structure, and H/D exchange, Subcell. Biochem. 23 (1994) 363–403.
[35] R. Chehin, I. lloro, M.J. Marcos, E. Villar, V.L. Shnyrov, J.L.R. Arrondo, Thermal and pH-induced conformational changes of a beta-sheet protein monitored by infrared spectroscopy, Biochemistry 38 (1999) 1525–1530.
[36] D. Naumann, C. Schultz, U. Gorne-Tschelnokow, F. Hucho, Secondary structure and temperature behavior of the acetylcholine receptor by Fourier transform infrared spectroscopy, Biochemistry 32 (1993) 3162–3168.
[37] A. Barth, Infrared spectroscopy of proteins, Biochim. Biophys. Acta 1767 (2007) 1073–1101.
[38] N. Dave, V.A. Lorenz-Fonfria, G. Leblanc, E. Padros, FTIR spectroscopy of secondary-structure reorientation of melibiose permease modulated by substrate binding, Biophys. J. 94 (2008) 3659–3670.
[39] L.K. Tamm, S.A. Tatulian, Infrared spectroscopy of proteins and peptides in lipid bilayers, Q. Rev. Biophys. 30 (1997) 365–429.
[40] D.T. Jones, Protein secondary structure prediction based on position-specific scoring matrices, J. Mol. Biol. 292 (1999) 195–202.
[41] N. Toyran, B. Turan, F. Severcan, Selenium alters the lipid content and protein profile of rat heart: an FTIR microspectroscopic study, Arch. Biochem. Biophys. 458 (2007) 184–193.
[42] K. Fahmy, F. Jager, M. Beck, T.A. Zvyaga, T.P. Sakmar, F. Siebert, Protonation states of membrane-embedded carboxylic acid groups in rhodopsin and metarhodopsin II: a Fourier-transform infrared spectroscopy study of site-directed mutants, Proc. Natl. Acad. Sci. U. S. A. 90 (1993) 10206–10210.
[43] A. Barth, The infrared absorption of amino acid side chains, Prog. Biophys. Mol. Biol. 74 (2000) 141–173.
[44] H. Susi, D.M. Byler, Fourier-transform infrared study of proteins with parallel beta-chains, Arch. Biochem. Biophys. 258 (1987) 465–469.
[45] S. Sukumaran, K. Hauser, A. Rauscher, W. Mantele, Thermal stability of outer membrane protein porin from *Paracoccus denitrificans*: FT-IR as a spectroscopic tool to study lipid–protein interaction, FEBS Lett. 579 (2005) 2546–2550.
[46] J.L. Arrondo, N.M. Young, H.H. Mantsch, The solution structure of concanavalin A probed by FT-IR spectroscopy, Biochim. Biophys. Acta 952 (1988) 261–268.
[47] F. Dousseau, M. Pezolet, Determination of the secondary structure content of proteins in aqueous solutions from their amide I and amide II infrared bands. Comparison between classical and partial least-squares methods, Biochemistry 29 (1990) 8771–8779.
[48] S. Mukherjee, P. Chowdhury, F. Gai, Infrared study of the effect of hydration on the amide I band and aggregation properties of helical peptides, J. Phys. Chem. B 111 (2007) 4596–4602.
[49] G. Verdon, O. Boudker, Crystal structure of an asymmetric trimer of a bacterial glutamate transporter homolog, Nat. Struct. Mol. Biol. 19 (2012) 355–357.
[50] F. Scheirlinckx, V. Raussens, J.M. Ruysschaert, E. Goormaghtigh, Conformational changes in gastric H^+/K^+-ATPase monitored by difference Fourier-transform infrared spectroscopy and hydrogen/deuterium exchange, Biochem. J. 382 (2004) 121–129.
[51] F. Korkmaz, S. Koster, O. Yildiz, W. Mantele, In situ opening/closing of OmpG from *E. coli* and the splitting of beta-sheet signals in ATR-FTIR spectroscopy, Spectrochim. Acta A Mol. Biomol. Spectrosc. 91 (2012) 395–401.
[52] M. Granell, X. Leon, G. Leblanc, E. Padros, V.A. Lorenz-Fonfria, Structural insights into the activation mechanism of melibiose permease by sodium binding, Proc. Natl. Acad. Sci. U. S. A. 107 (2010) 22078–22083.
[53] C.J. Tsai, K. Khafizov, J. Hakulinen, L.R. Forrest, R. Kramer, W. Kuhlbrandt, C. Ziegler, Structural asymmetry in a trimeric Na(+)/betaine symporter, BetP, from *Corynebacterium glutamicum*, J. Mol. Biol. 407 (2011) 368–381.
[54] H. Krishnamurthy, E. Gouaux, X-ray structures of LeuT in substrate-free outward-open and apo inward-open states, Nature 481 (2012) 469–474.